AD-A225 158

DTIC FILE COPY

MT-CWR-090-012

ANNUAL REPORT

(2)

Fundamental Concepts of Wettability and Interfacial Bond Strength in Aluminum Matrix, SiC-reinforced Composites

DTIC
ELECTE
AUG 07 1990
S D
D

Submitted to:
Dr. Steven Fishman
Office of Naval Research
Arlington, Virginia 22217

Submitted by:
Glen R. Edwards and David L. Olson
Center for Welding and Joining Research
Colorado School of Mines
Golden, Colorado 80401

July, 1990

DISTRIBUTION STATEMENT A
Approved for public release;
Distribution Unlimited

This program supported by the Strategic Defense Initiative Office/Innovative Science and Technology under ONR contract N00014-88-K-0500.

TABLE OF CONTENTS

		Page
1.0	PROJECT SUMMARY.	3
	1.1 Surface Energy Measurement.	3
	1.2 Wettability Predictions	3
	1.3 Interfacial Bond Energies	3
2.0	LIST OF ACCOMPLISHMENTS.	4
	2.1 Graduate Thesis	4
	2.2 Publications.	4
	2.3 Published Abstracts	5
3.0	SURFACE ENERGY MEASUREMENTS.	7
	3.1 Differential Reflectometry.	8
4.0	WETTABILITY PREDICTIONS.	18
	4.1 Background.	18
	4.2 Reactive Interface.	19
	4.3 Oxide Defect Structure.	21
5.0	INTERFACIAL BOND STRENGTH.	32
	5.1 Background.	32
	5.2 Punch Shear Tests (Al/SiC).	34
	5.3 Interfacial Strength of the Al/SiC Bond	38
	5.4 Punch Shear Results (Al/SiC).	43
	5.5 Comparison to Model (Pure Aluminum Matrix). . . .	45
	5.6 Punch Shear Results (Aluminum Alloy Matrix) . . .	47
	5.7 Comparison to Model (Aluminum Alloy Matrix) . . .	48
6.0	REFERENCES	52

STATEMENT "A" Per Dr. Steven Fishman
ONR/Code 1131
TELECON 8/6/90 VG

Accesion For
NTIS CRA&I ☑
DTIC TAB ☐
Unannounced ☐
Justification
By per call
Distribution /
Availability Codes
Dist | Avail and / or Special
A-1

1.0 PROJECT SUMMARY

Research accomplishments on this project during the last academic year are in three distinct areas: a) surface energy measurements, b) wettability predictions, and c) interfacial bond energies.

1.1 Surface Energy Measurement

Differential optical reflectance was used to measure the optical transitions in aluminum and its alloys. The semi-empirical correlation developed earlier was used to calculate the surface energy from the measured transition energies. Predicted surface energies, using the model, were in close agreement with experimentally determined surface energies found in the literature.

1.2 Wettability Predictions

Wettability studies are based on surface tension measurements from the capillary rise experiment. A mechanism, assuming a defect-rich oxide interlayer at the interface, was proposed to explain the non-wetting behavior of the Al/SiC system.

1.3 Interfacial Bond Energies

The measured surface energies were used to predict the interfacial bond energies using a work of decohesion model. Punch shear tests were used to make relative determinations of bond strengths for several aluminum alloy/SiC systems. The predicted bond energy trends correlated well with the observed bond strengths.

2.0 LIST OF ACCOMPLISHMENTS

2.1 Graduate Thesis

1. Maxwell, P.B., "The Infiltration Behavior of Aluminum into Silicon Carbide Compacts", CSM M.S. Thesis No. T-3396, Colorado School of Mines, April 1987.

2. Seitz, J.D., "The Infiltration Kinetics of Silicon Carbide Reinforced Aluminum Matrix Composites", CSM M.S. Thesis No. T-3614, Colorado School of Mines, December 1988.

3. Lanning, B.R., "A Method for Predicting Wettability and Interfacial Bond Strengths at Metal/Ceramic Interfaces", CSM Ph.D. Thesis No. T-3875, Colorado School of Mines, April 1990.

2.2 Publications

1. Martins, G.P., Olson, D.L., and Edwards, G.R., "Modeling of Infiltration Kinetics of Liquid Metal Processing of Composites", Met. Trans., Vol. 19B (1988), pp. 95-111.

2. Seitz, J.D., Edwards, G.R., Martins, G.P., and Campbell, P.Q., "Infiltration Mechanisms and Kinetics of Liquid Aluminum Infiltration of α-SiC Compacts", Proceedings, Interfacial Reactions in Composites, AIME, Anaheim, CA, February 1990.

3. Maxwell, P.B., Martins, G.P., Olson, D.L., and Edwards, G.R., "The Infiltration of Aluminum into Silicon Carbide Compacts", Met. Trans. A, in press.

4. Lanning, B.R,. Furtak, T., and Edwards, G.R., "A Method for Predicting Metal-Ceramic Interfacial Bond Energies", Journal of Materials Research, in press.

5. Lanning, B.R., Edwards, G.R., and Olson, D.L., "Wettability of Aluminum and Aluminum Alloys on SiC", submitted to Scripta Met.

6. Chidambaram, P.R., Lanning, B.R., and Edwards, G.R., Wettability Predictions at Metal-Ceramic Interfaces", to be published.

2.3 Published Abstracts

1. Edwards, G.R., Martins, G.P., Olson, D.L., Lanning, B.R., and Maxwell, P.B., "Infiltration Kinetics and Interfacial Bond Strengths in Aluminum Matrix-Silicon Carbide Composites", Conference Proceedings, 8th Annual MMC Meeting, Park City, UT, MMCIAC, pp. 219-242, 1986.

2. Lanning, B.R., Furtak, T., and Edwards, G.R., "Determination of Interfacial Bond Energies Using Modulation Reflectometry", Proceedings, Advanced Materials Conference II, Denver, March 6-9, 1989, CATI-MRS, pp. 315-318, 1989.

3. Lanning, B.R., Edwards, G.E., and Olson, D.L., "A Semi-Empirical Model for Predicting Properties of the Al/SiC Interface", Proceedings, Eleventh Annual Discontinuously Reinforced MMC Working Group Meeting, Park City, UT, MMCIAC No. 716, pp. 441-458, 1989.

4. Seitz, J.D., Campbell, P.Q., Edwards, G.R., and Martins, G.P., "Infiltration Characteristics of Aluminum-Silicon-Carbide Campsites", Proceedings, Eleventh Annual Discontinuously Reinforced MMC Working Group Meeting, Park City, UT, MMCIAC, No. 716, pp. 459-488, 1989.

3.0 SURFACE ENERGY MEASUREMENTS

It has been well established that the surface energy is a fraction of the bulk cohesive energy. Realizing this interdependence, the detailed spectroscopic theory developed by Phillips and Van Vechten to calculate cohesive energy and heat of formation of semiconducting ceramics, can be used to measure surface energies, γ^{so}:

$$\gamma^{so} = \gamma_o^{so}[1-a^{-1/2} f(AB)] \qquad (1)$$

where: γ_o^{so} = scaling factor, a = lattice parameter, and f(AB) = fractional ionicity.

Similar direct correlation between electronic parameters and the cohesive energy in metals is currently available. Consequently, such an empirical equation was developed as a part of this study.

$$\gamma^{so} = C_1 (1+V_2)^{1/2} (h\omega_p)^{1/2} n^{2/3} \qquad (2)$$

where: V_2 = p-s transition energy, ω_p = plasma frequency, and n = electron density.

Details of this model and a comparison between predicted and measured surface energies were discussed in the previous reports (1,2). Experimental procedures used to measured V_2, and the methodology adopted to calculate surface energies with particular reference to aluminum magnesium alloys, are described in the following sections.

3.1 Differential Reflectometry

The optical technique of differential reflectometry was used to measure the interband transition energies, V_1, V_2, and V_3 in the Al-Li, Al-Mg, and Cu-Zn alloys. The theory of this differential technique was presented in previous reports (2).

The principle involved is simple; unpolarized, monochromatic light from the source strikes the samples at near normal incidence. The reflected light is electronically processed to yield the reflectance ratio, $\Delta R/R = 2(R_1-R_2)/(R_1+R_2)$. Owing to the nature of the differential reflectance technique, the effects of instrument parameters, such as background noise or intensity fluctuations, are effectively eliminated.

A positive feature of differential reflectance is the sensitivity of the technique to surface properties. Conventional optical spectroscopies are used for the study of bulk properties because of the great penetration depth of light in solids (10-50 nm for metals and ~10^7 nm for pure SiC). However, since the principle of differential reflectance is to compare the reflectance of a sample with the reflectance of the same sample slightly modified, the perturbation to the second sample can be made to enhance features of the electronic structure at the surface. The relative reflectance change $\Delta R/R$, for this case, will then relate to the change in electronic structure at the surface.

A schematic of the differential reflectance apparatus is shown in Figure 1. Light from a focused xenon source (XBO, 150

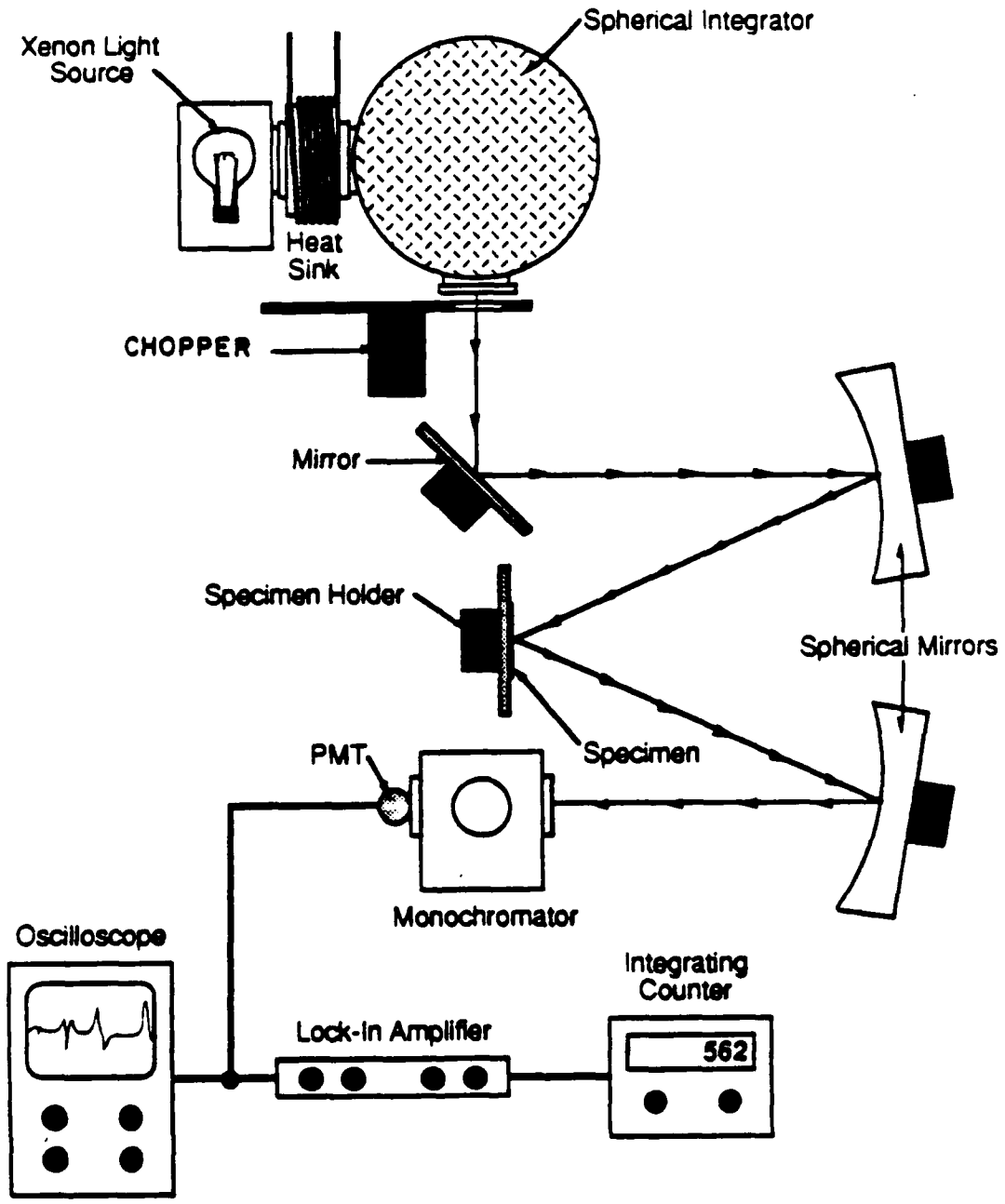

Figure 1. Schematic illustration of differential reflectance apparatus.

W/S) was directed into an integrating sphere which balances or equalizes the spatial intensity of the light. Light exits from the sphere out of two 3.2-cm holes, passes through a chopper (at 47 Hz), and refocuses onto the sample surfaces at near normal incidence (spot area equal to ~16 mm^2). The two samples (2-4 pct compositional differences) are mounted side by side in a bakelite mount and the two parallel light beams strike the samples at alternate intervals preset by the chopper frequency. The reflected light from both samples then passes into a monochromator and finally into a photomultiplier tube, PMT (Hamamatsu R758), which detects the signal. The light at the entrance slit to the monochromator is defocused to reduce special dependence within the monochromator and PMT.

The signal from the PMT is sent to an oscilloscope and to a lock-in amplifier (ITHACO; Dynatrac 391A) which yields an output proportional to $\Delta R = R_1 - R_2$. An oscilloscope allows a direct measurement of the normalized difference in the reflectivities of the two samples and an observation of whether or not the light beam remains an equal amount of time on both samples.

The output voltage from the lock-in amplifier is then sent through a voltage-frequency convertor and then to an integrating counter (i.e. measurement is recorded in counts). Even though the overhead light did not affect the PMT output, the reflectance measurements were performed in the dark.

Copper zinc alloys were used initially to calibrate the system. The copper-zinc alloys were prepared from (99.999%

purity) copper and zinc shot (~1.3 mm), melted at 1100°C for two hours and homogenized at 900°C for ~10 days in a vacuum furnace.

The aluminum-magnesium and aluminum-lithium samples were prepared and cast in a controlled argon atmosphere glove box. Purity of the aluminum was 99.95 wt pct. After casting, the samples were then warm rolled (~300°C) to 50 pct reduction. In contrast to the copper alloys, precipitation occurred in the aluminum-magnesium alloys, although the precipitates were uniformly dotted throughout the grains. The aluminum-lithium alloys were relatively free of precipitates albeit the grain size was larger than in the aluminum-magnesium alloys.

The samples were mounted side by side in bakelite, and polished to 1μm using standard metallographic procedures. For the aluminum alloys, the final polishes were with diamond paste, rather than with water-immersed compounds, to minimize oxidation. After polishing, the samples were ultrasonically cleaned and rinsed in methanol.

The mounted and polished samples were then clamped into an adjusted stage. Lateral and vertical movements in the stage were necessary to position the optical beams onto the samples and select specific areas on the samples. Prior to acquiring a spectrum, the alignment of the second spherical mirror in the reflectometer was finely adjusted to balance the output of the positive (0°) and negative (180°) responses of the lock-in amplifier.

The procedure for acquiring a spectrum consisted of stepping through the wavelength range of interest and recording the number of counts (equal to $\Delta R/R$). At each wavelength, the input voltage to the PMT was adjusted to yield a fixed present output voltage from the PMT. A number of points in the spectrum were rechecked in the reverse scan direction.

Differential reflectometry of aluminum and aluminum alloys was found to be more difficult than reflectometry on copper-zinc alloys.

It was found that the aluminum alloys were: 1) influenced by the xenon light source over the energy range of interest, 2) dependent on the technique of preparation prior to the final polish, and 3) very sensitive to the final polish. Careful sample polishing and signal processing techniques were used to minimize such interference. As long as the electronic structure and thickness of the surface oxides of the two samples are the same, then the normalizing nature of the differential technique eliminates the effect of the oxide.

The reflectance spectra for the 12 wt pct (6.05/18%) Cu-Zn alloy is shown in Figure 2. The peaks and 'crossover' points match exactly (to within 0.01 ev) the reported spectra of Hummel for this alloy. The lineshape is also identical with the work of Hummel et al. (4).

Having established the sensitivity and the reproducibility of the reflectometer with the previous copper-zinc alloys, the aluminum alloys of interest were then investigated.

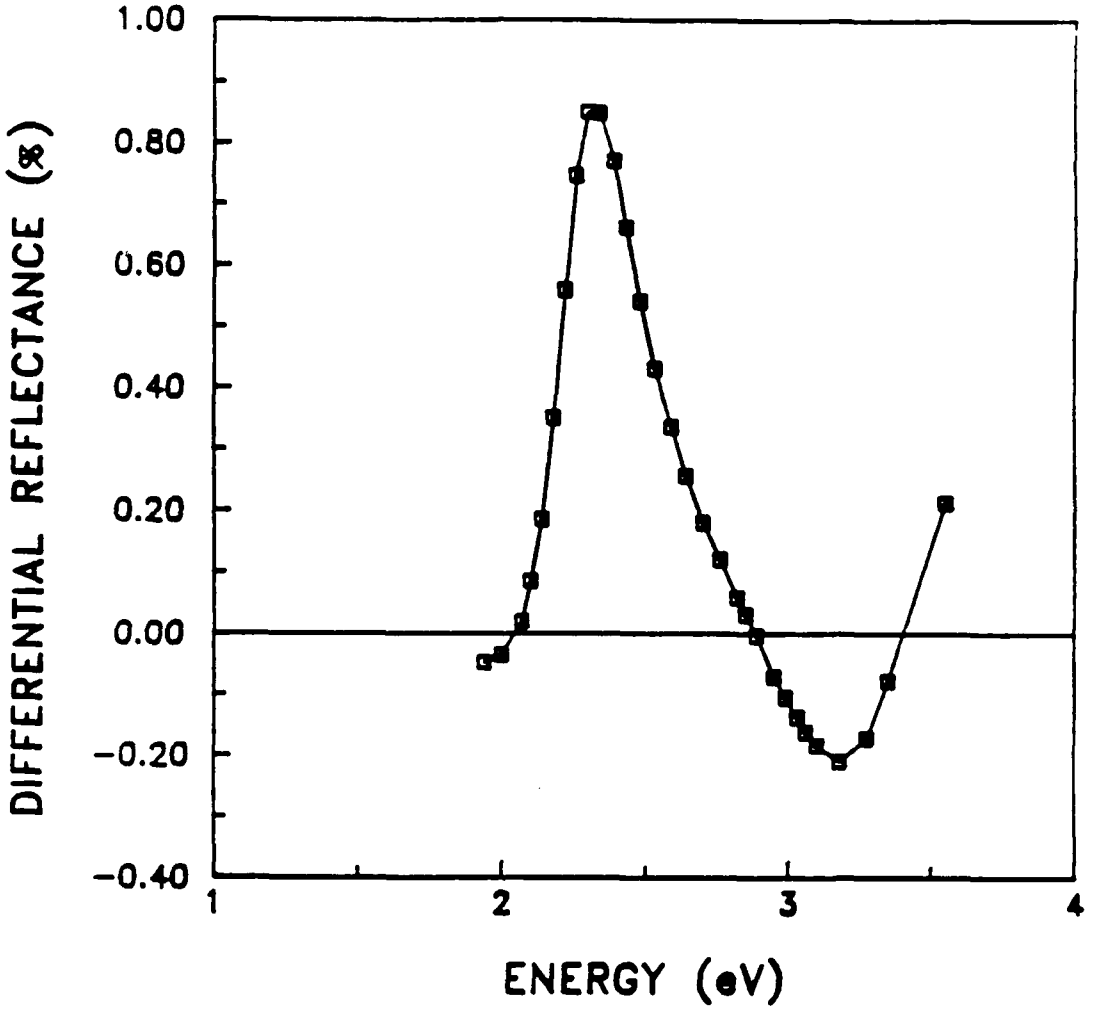

Figure 2. Reflectance spectra for copper-12 percent Zn alloy.

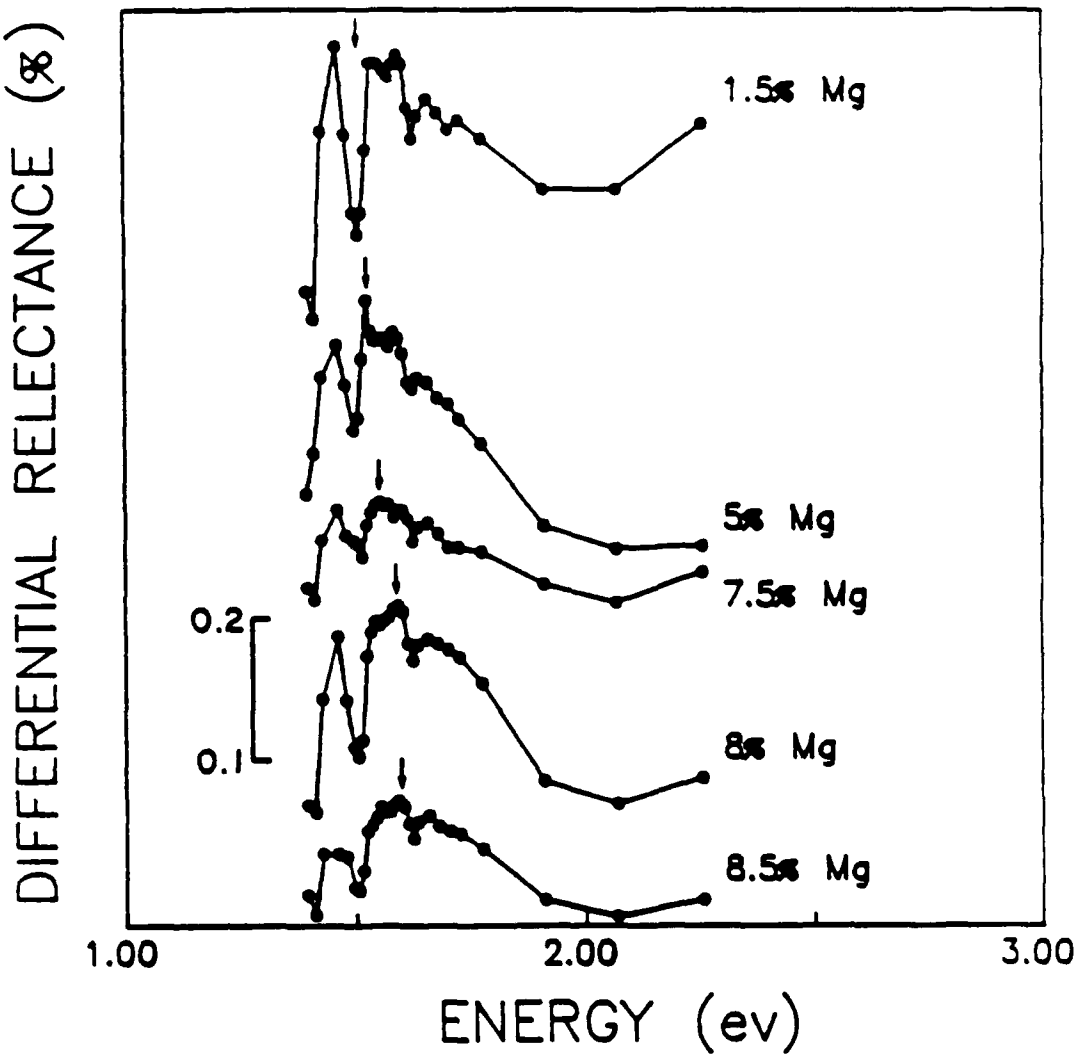

Figure 3. Reflectance spectra for aluminum-magnesium alloys.

Differential spectrum for aluminum-magnesium alloys is shown in Figure 3. An important feature of the spectrum is the characteristic parallel-band absorption peak which occurs at around 1.5 ev (this corresponds to a wavelength of 828 nm). The rapid drop off at the low energy is due to the detectability limit of the detector and the inverted spike at 1.5 ev is from the xenon light source. For identical specimens, the response was essentially flat with no observable peak.

In comparison to other reflectance work that was done at low temperatures (4°K), where the absorption peak was observed at ~1.59 ev (5), the observed room temperature peak at 1.5 ev is consistent with the shift in temperature that would be expected to occur. The height of the peak also demonstrates the sensitivity of the technique.

Although samples were immediately tested after polishing to minimize oxidation/contamination, the lag time, between the final polish and the reflectance measurement, did not appear to influence the position of the peak. Increasing lag times (i.e. hours or even days) only seemed to decrease the intensity of the peak.

The magnesium concentration listed is the average of the two samples and the difference in concentration between the two samples was no more than four percent. As the magnesium concentration increased, the transition energy also increased.

An increase in transition energy with magnesium concentration could only be explained by the formation of

precipitates in the matrix. Precipitates were found in the microstructure of all these alloys. Since the room temperature equilibrium solubility limit of magnesium in aluminum is ~1 5 pct, it was not possible to prevent the formation of precipitates with the sample preparation procedures used in this study.

The observed transition energies from these measurements were then used to calculate the predicted surface energies according to Equation 2, and the results are given in Table 1. With increasing magnesium concentration, the surface energy is predicted to decrease slightly. Although the calculated electron concentration and plasma frequency decrease with increasing magnesium concentrations, these effects are offset slightly by the positive change in the transition energy.

TABLE 1 - Predicted Surface Energies of Magnesium and Lithium Using Measured Optical Transition Energies from the Model

Alloy	Concentration (atomic percent)	Transition Energy (ev)	Surface Energy J/m^2
Al-Mg	0	1.5	1.084
	1.5	1.52	1.083
	5	1.55	1.075
	8	1.58	1.069
Al-Li	0	1.5	1.084
	2.2	1.51	1.063
	4	1.5	1.046
	5.5	1.5	1.031

4.0 WETTABILITY PREDICTIONS

4.1 Background

Wettability, in this study, was characterized with the parameter, $\gamma_{lv}\cos\theta$; if $\gamma_{lv}\cos\theta$ was positive (0<90 degrees) or negative (0>90 degrees), the system was respectively, either wetting or non-wetting. The value $\gamma_{lv}\cos\theta$ is equivalent to, according to the Young equation, the difference between γ_{sv} and γ_{sl}. For the non-reactive case, the magnitude of γ_{sl} is between γ_{sv} and γ_{lv}. In the event that an oxide or contaminant is present at the interface, γ_{sl} can be greater than both γ_{sv} and γ_{lv}. In any event, the magnitude of γ_{sv} is always greater than γ_{lv} for the non-reactive case. For the case when the substrate and liquid are reactive, the free energy of the reaction enhances the driving force for wetting by decreasing the magnitude of γ_{sl}, and wetting will occur regardless of whether γ_{sv} is greater or less than γ_{lv}.

The fundamental development of both γ_{sv} and γ_{sl} have been presented earlier in terms of fundamental parameters. The value of γ_{sv} for the SiC substrate, in this wettability discussion, is taken from the literature. Takai et al. (6) have theoretically determined the surface energies for different β-SiC surfaces at T=260°K. Since reported surface energy data for SiC is limited (only one measurement for the surface energy of β-SiC (111) surface was reported), an average energy was determined from data of Takai.

Using the fact that the total surface free energy of a crystal is equal to the sum of the products of the specific surface energy of each crystal face times the area of each crystal face, an average surface free energy was calculated. Surface areas of the crystal faces were related to multiplicity factors. The average surface energy for pure SiC was therefore assumed to be 1.8 J/m^2. Without available surface energy data for α-SiC, the surface energy for α-SiC was approximated by the value of surface energy for β-SiC.

Changes in the wetting behavior for different alloy additions are primarily related to changes in the γ_{sl} term. As shown before (2):

$$\gamma_{sl}^{AB} = 2.5 \times 10^{-9}/V^{2/3} \left[L_f^A (1-T/T_m) + \Delta H_m^{AB}\right] \qquad (3)$$

where T_m is the melting point of the substrate and V_m is the molar volume. The first term on the right hand side of the equation pertains to the solid substrate and the second term, ΔH^{AB} is a measure of the degree of interaction or non-interaction; the interaction term may be positive or negative, but rarely equal to zero.

4.2 Reactive Interface

The Al/SiC system is unique in that both reactive and non-reactive situations may occur. If pure aluminum were to contact

pure SiC, then aluminum carbide would immediately form according to the following reaction:

$$\frac{4}{3}Al_{(1)} + SiC_{(s)} \rightarrow \frac{1}{3}Al_4C_{3(s)} + Si_{(1)} \qquad (4)$$

The standard enthalpy for this reaction is negative. Since the magnitude of the first term in the γ_{sl} expression is less than the free surface energy, γ_{sv}, the overall difference between γ_{sv} and γ_{sl} will be positive and therefore aluminum will wet SiC.

In the results from the capillary rise experiments, aluminum did not wet SiC. There is corroborating evidence in the literature that aluminum does not wet SiC spontaneously. Spontaneous wetting of SiC by aluminum was reported to occur above ~950°C; whereas, at temperatures below 900°C, wetting did not begin prior to an incubation period of at least a few seconds.

Analogous to the process of infiltration, there is an incubation time in the equilibrium wetting tests prior to wetting of SiC by liquid aluminum, and it is the behavior of this incubation period that influences the observed wettability. In the event oxides or impurities are present at the interface, wetting may or may not occur depending on the stability of these contaminants. It is believed that oxides are responsible for the observed incubation periods in this system. A mechanism is therefore proposed in the next section which describes the non-wetting condition at the transition to a wetting condition.

4.3 Oxide Defect Structure

Adsorbed oxygen or oxides on the surfaces of aluminum or SiC significantly change the wetting behavior of aluminum on SiC. Aluminum oxide readily forms on the surface of molten aluminum at pressures greater than 10^{-6} atm. and is invariably part of the aluminum/SiC interface. Although the oxide thicknesses may only be 2-5 nm, continuous oxides are known to form with oxide thicknesses of only 2-3 nm because of a positive molar volume change from aluminum to aluminum oxide .

Upon formation of a continuous oxide film, the transport of aluminum to the surface could occur only by the process of diffusion through this 'solid state' film. Since lattice diffusion rates of aluminum in Al_2O_3 are on the order of 10^{-20} $cm^2/sec.$, pure aluminum does not transport to the metal/ceramic surface by this mechanism. A proposed configuration for the Al/SiC interface, most commonly encountered when silicon carbide substrates are subjected to liquid aluminum, is shown in Figure 4.

The aluminum oxide film (~2-5 nm) forms an impermeable barrier between the molten aluminum and the SiC substrate. On the other side of the interface, SiC may or may not form an oxide, and in this discussion, both the oxide and oxide-free surfaces will be treated separately.

The proposed interface configuration shown in Figure 4, is essentially an aluminum oxide in contact with either a SiC or SiO_2 (oxygen adsorbed on SiC) substrate. Wettability then, is

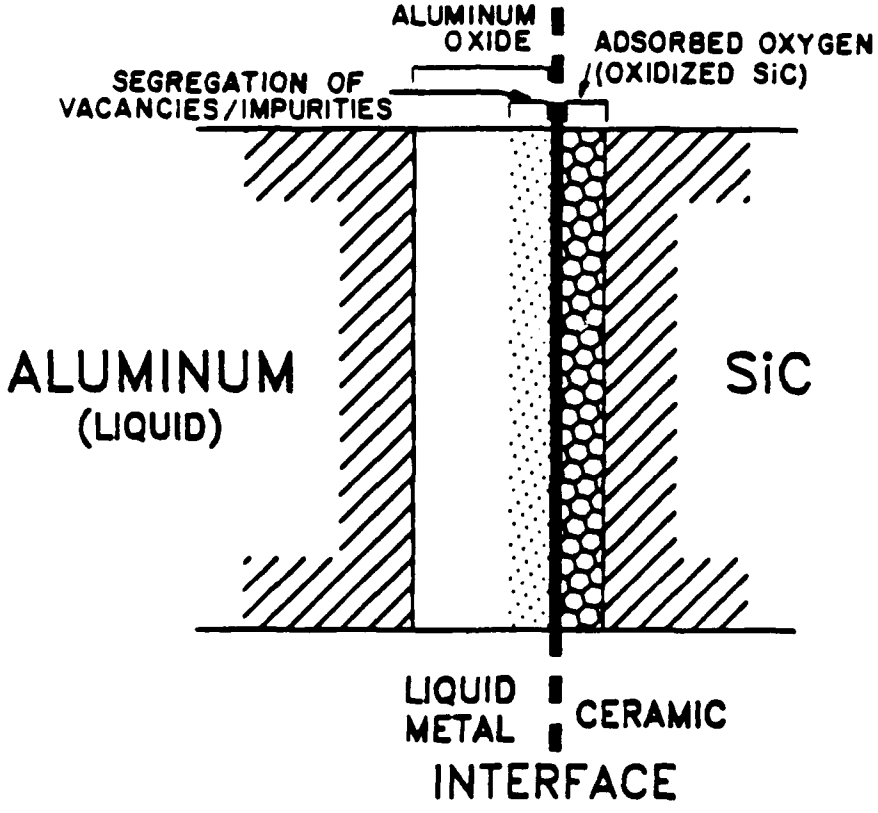

Figure 4. Schematic configuration of a proposed liquid aluminum/silicon carbide interface for a non-reactive case.

characterized by the interaction of these "non-reactive" oxide surfaces. With respect to the γ_{sl} equation (Equation 3), the interaction term is related to the enthalpy of mixing, ΔH_m. The solubilities for metals in contact with ceramics are very low. Heats of solution or enthalpies of mixing in ceramic systems can be evaluated in terms of the defect structure of the lattice. The lattice in this case will refer to the aluminum oxide skin in the interface region.

Although electronic defect concentrations could be used to determine heats of solution, only atomic defects are considered for this model. The primary atomic defects in this structure are vacant lattice sites and the substitutional impurities on cation sites. The formation energies of intrinsic defects, such as Schottky disorders, are given in Table 2. Along with these values are substitutional doping energies (in α-Al_2O_3) for the solutes used in this study. These calculated values are from Mackrodgt (7) and the cation formation energies are calculated from the reported heats of solution.

Three conditions are considered: 1) pure aluminum (or pure aluminum with silicon additions), 2) pure aluminum with magnesium additions, and 3) pure aluminum with lithium additions. The pure aluminum case represents intrinsic defects in the Al_2O_3 film and the aluminum alloys add substitutional defects into the Al_2O_3 film. In the formulation of the reactions for the defect oxide structure, the reaction for a silicon addition would be the same as the pure aluminum case. Silicon additions merely shift the

TABLE 2 - Formation Energies of α-Al_2O_3 Defect Structure

Species	Formation Energy (ev/atom)
V_o	5.0*
V_{Al}	5.0
Si_{Al}	1.8
Mg_{Al}	0.7
Li_{Al}	0.9

direction or balance of equilibrium by changing the silicon activities.

The proposed reactions and corresponding heats of solution, are given below:

1. Pure aluminum metal -

$$3Si + 3O_2 \xrightarrow{Al_2O_3} 3Si^{\bullet}_{Al} + V^{'''}_{Al} + 6O_o \qquad (5)$$

ΔH_m = 337 kJ/mole Si

2. Aluminum with magnesium addition -

$$Si + O_2 + MgO \xrightarrow{Al_2O_3} Si^{\bullet}_{Al} + Mg^{'}_{Al} + 3O_o \qquad (6)$$

ΔH_m = 243 kJ/mole Si

3. Aluminum with lithium addition

$$12Si + 12O_2 + 3Li_2O \xrightarrow{Al_2O_3} 12Si^{\bullet}_{Al} + 6Li^{''}_{Al} + 27O_2 \qquad (7)$$

ΔH_m = 219.3 kJ/mole Si

In these equations, ΔH_m is the heat of solution, $V^{'''}_{Al}$ is a negatively charged (3$^-$) cation vacancy, $Mg^{'}_{A}$ is a negatively charged (1$^-$) cation substitutional solute, $Li^{''}_{Al}$ is a negatively charged (2$^-$) cation substitutional solute, and $Si^{\bullet}_{Al}$ is a positively charged (1$^+$) cation substitutional solute. The same result can be drawn when the silicon is present as either SiC or

SiO_2 on an alumina substrate in the presence of oxygen. Heats of solution from these reactions are then used to calculate the second term of the γ_{sl} expression.

For the case of aluminum (aluminum oxide) on pure, unoxidized SiC, wettability ($\gamma_{lv}\cos\theta$) is equal to the free surface energy of pure SiC minus the solid/liquid interfacial energy. For SiC, γ_{sl} is equal to 1.8 J/m^2. The terms in γ_{sl} are proportional to L_f, the latent heat of fusion of the substrate, and ΔH_m, where ΔH_m is given in the previous section.

Since SiC does not melt, L_f is approximated by the heat of dissociation of SiC; i.e. the formation of silicon vapor and graphite. The calculated heat of dissociation for SiC is equal to 113.8 kcal/mole (8). Therefore, the solid/liquid interfacial term for aluminum in contact with SiC is equal to:

$$\gamma_{sl} = 2212\,[1-T/3500] + 967 \qquad (8)$$

where γ_{sl} is in mJ/m^2 and T is in degrees Kelvin.

If the SiC surface has been oxidized, a similar calculation for the wetting tendency of this substrate by liquid aluminum can be made by utilizing the surface free energy, γ_{sv}, for SiO_2. From the literature (9);

$$\gamma_{sv}(SiO_2) = 307 + 0.031\,(T - 2073) \qquad (9)$$

The latent heat of fusion, L_f, for SiO_2 is 2.29 kcal/mole at the melting point (1996 K). For the case of pure aluminum on an

oxidized SiC substrate, the interfacial energy is therefore equal to:

$$\gamma_{sl} = 27.4\ (1 - T/1996) + 967 \qquad (10)$$

Both experimental results and the predicted results from the model (for pure SiC) are plotted in Figure 5. Experimental and predicted values are plotted as solid and dashed lines respectively.

The proposed model correctly predicts the effect of alloy additions on the wetting behavior. Even the experimentally measured slopes are nearly the same as the calculated slopes. As discussed in the previous section, the slope of the line in a $\gamma_{lv}\cos\theta$ versus temperature plot appeared to relate to the extent of SiC oxidation at the Al/SiC interface. The deviation of the experimental slopes from the calculated slopes suggests that there was some degree of oxidation at the SiC surface; the experimental slopes were located between the two model cases, SiO_2 and SiC surfaces, presented earlier.

The results from this study also suggest that additions of silicon to aluminum will not affect significantly the wetting of SiC by aluminum. Although wetting by an Al-2%Si alloy appeared more favorable than wetting by pure aluminum, the effect of silicon is mainly to control the equilibrium carbide reaction by driving the equilibrium to the reactants side and preventing formation of the carbide.

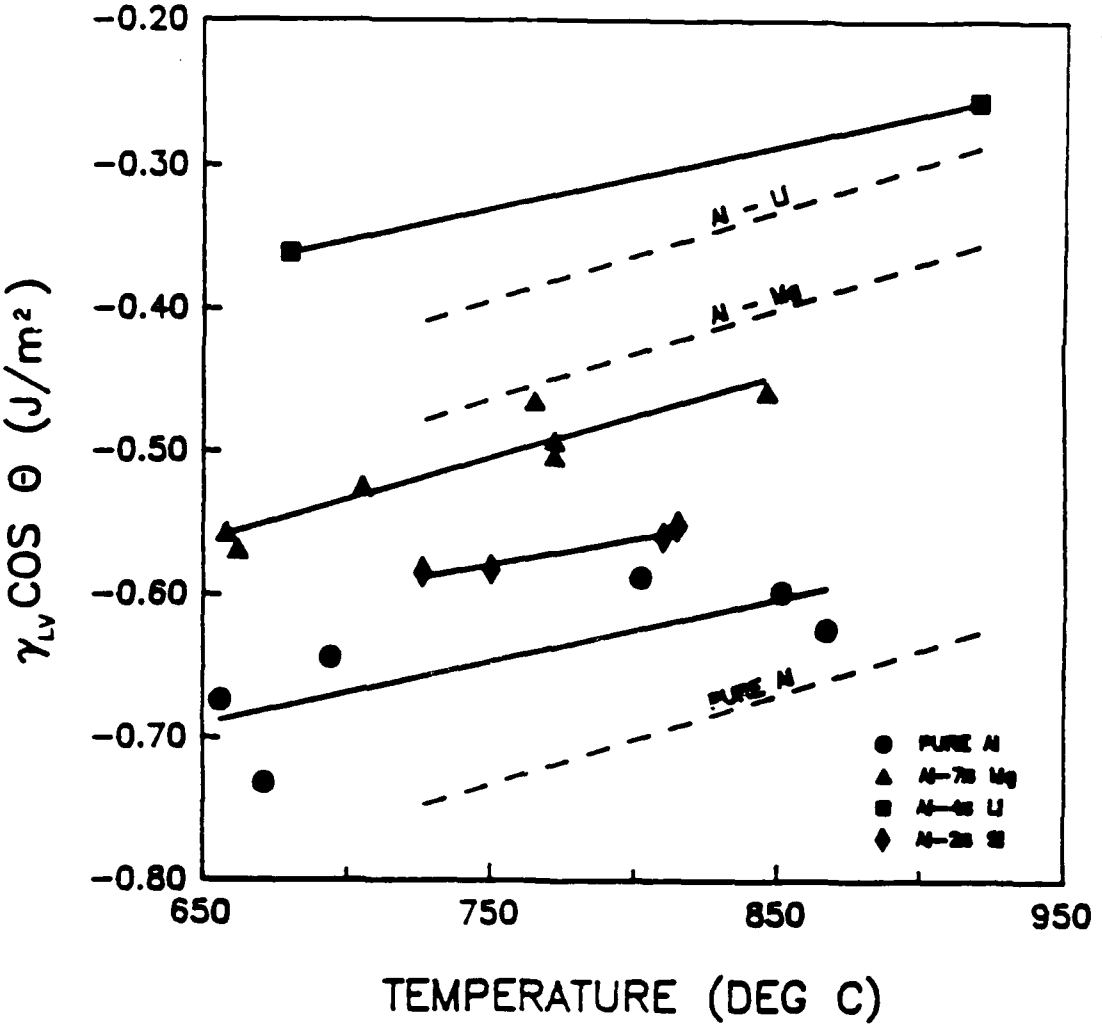

Figure 5. Comparison between theoretical and experimental value of $\gamma_{lv}\cos\theta$, plotted versus temperature.

Finally, a speculative explanation is given for the experimentally observed transition from a non-wetting to a 'reactive' wetting system. The formation of an aluminum oxide film was shown to prevent wetting in the case just presented. The transition from non-wetting to wetting behavior hinges on the chemical reduction or mechanical degredation of this oxide. Since aluminum oxide is thermodynamically stable and not easily reduced, there does not appear to be a chemical driving force for penetrating the barrier oxide film and allowing aluminum metal to react with SiC. Therefore, for aluminum to wet or react with SiC, another mechanism, such as physical or mechanical break-up of the protective film, must occur.

Above 900 K, the growth rate of the refractory oxide, Al_2O_3, on pure aluminum is linear. This type of reaction requires open pathways between the oxygen source and the liquid metal. The development of flaws in the 'amorphous' oxide layer would provide such pathways or channels. Recrystallization of Al_2O_3 phases, which would create new interfaces, have been observed at the wetting temperature of this investigation. The creation of interfaces in the oxide film would provide a method by which aluminum could channel to the ceramic interface. If the oxide layer thickness was only 3-5 nm, the channel forming rate would be of the same order of magnitude as the observed transition (incubation) times.

A pictorial representation of the 'channeled' aluminum oxide film in the wetting system is shown in Figure 6. For any

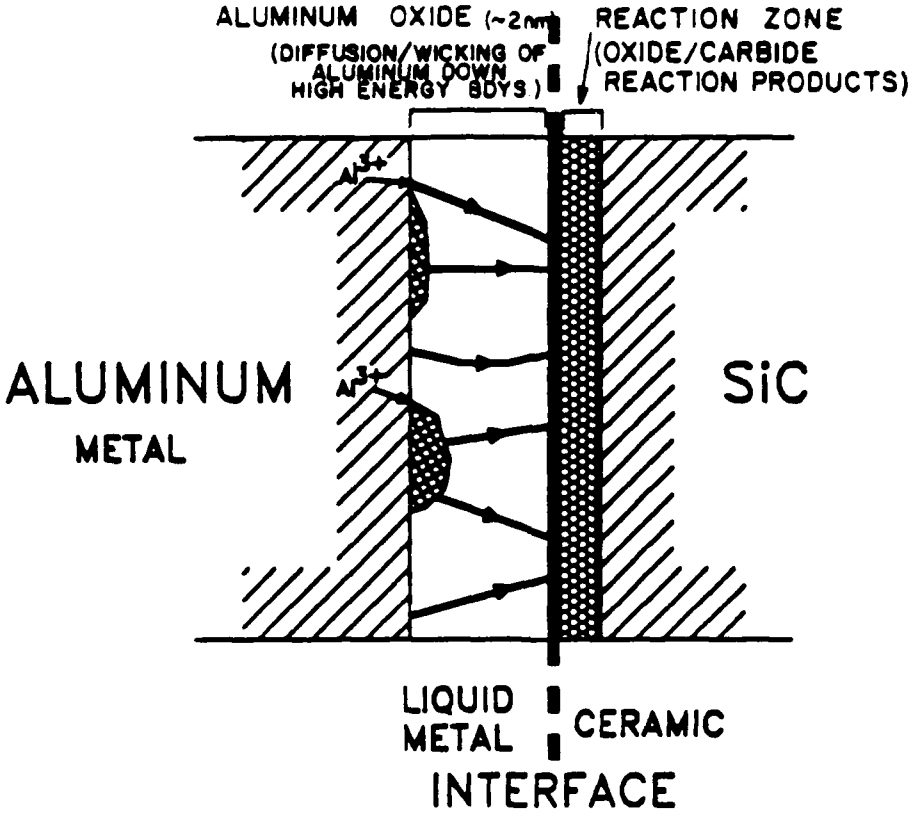

Figure 6. Schematic configuration of the liquid aluminum/silicon carbide interface for a reactive case.

strength to develop at the interface upon cooling, aluminum would then channel from the bulk to the interface and react with the SiC to form a carbide (shown as a reaction zone). This same conceptual model provides a basis for explaining the observed interfacial bond strengths in the next section.

5.0 INTERFACIAL BOND STRENGTH

5.1 Background

In binding or cohesive energy type calculations, the total energy consists of the energy of the pure components and energies characterizing the various types of interactions between the pure components. Evaluation of this interaction energy between the two components is paramount to an accurate determination of the interfacial energy. In this study, the same approach in calculating the interfacial energy for the solid/liquid case is used for the solid/solid case. The equilibrium sessile drop analogy is valid in the solid/solid case where the solid metal (at temperatures ~$0.7T_m$) assumes an equilibrium particle shape of minimum surface free energy.

In addition to the internal energy of the substrate and the chemical interaction, the effects from geometric misfit (between the lattice) and the associated strain energy are included in the γ_{ss} case. Neglecting the strain energy for this exercise, the metal/ceramic interfacial energy, γ_{ss}, would be:

$$\gamma_{ss}^{AB} = AL_f^A [1-T/T_m] + A\Delta H_f + 0.15(\gamma_{sv}^A + \gamma_{sv}^B) \qquad (11)$$

where the parameters have the same meaning as presented earlier for the γ_{sl} case.

Since one purpose of this study was to compare measured interfacial strengths with predicted strengths from the surface energy model, the cohesive energy will be defined in terms of a

simple work of fracture, or energy of decohesion expression. For a metal/ceramic interface, the energy of decohesion (α work adhesion) would then be:

$$E_a = \text{Work of Decohesion} = \gamma_{sv}^{A} + \gamma_{sv}^{AB} - \gamma_{ss}^{AB} \qquad (12a)$$

where γ_{sv} is the free surface energy and γ_{ss} is the interfacial energy.

The theoretical stress to separate the metal and ceramic interface would therefore be (10):

$$\sigma_{max} = \frac{E_y(E_a/2)]^{1/2}}{a} \qquad (12b)$$

where E_y is the elastic modulus, a is the atom spacing, and E_a is proportional to the work of decohesion.

At some point, a value for the lattice spacing is necessary to calculate the theoretical interface strength. If the compositional changes due to alloy additions are minimal, then it will be assumed that the relative trends in the measured strengths with alloy additions will reflect changes in the surface and interfacial energies and not the lattice spacing term, a. Therefore, the calculated and measured strengths at the interface will be normalized with respect to a reference strength, such as the strength of the pure metal matrix.

Though approximations and simplifications are used in evaluating the metal/ceramic bond strengths, the focus in this

study is to develop a general method for evaluating the electronic nature of each of the surfaces separately and use this information to predict the subsequent interfacial properties. Specific atomistic calculations may not provide insight into the observed character of general metal/ceramic interfaces.

5.2 Punch Shear Tests (Al/SiC)

A punch shear test was used to determine the relative strengths of different Al/SiC interfaces. Although this method may not provide an accurate measure of the absolute interfacial strength, it is an effective way to characterize relative changes in the interfacial strengths.

One other important feature of this test was the localization of stress along the metal/ceramic bond plane. Since the interaction between the molten aluminum and SiC was incomplete, resulting in fractional areal contact, the load at the interface was carried by a reduced cross-sectional area. The fracture path was then concentrated along the metal/ceramic bond line; thereby increasing the probability of fracture along this line.

A jig was constructed to punch the ceramic core out of a pre-cut aluminum/SiC disc and a schematic of the jig is shown in Figure 7. This jig was mounted in the grips of an Instron tensile testing machine. As the Instron crossheads moved apart, the punch sheared the ceramic away from the metal matrix and a measurement of the shear force was recorded on the Instron strip

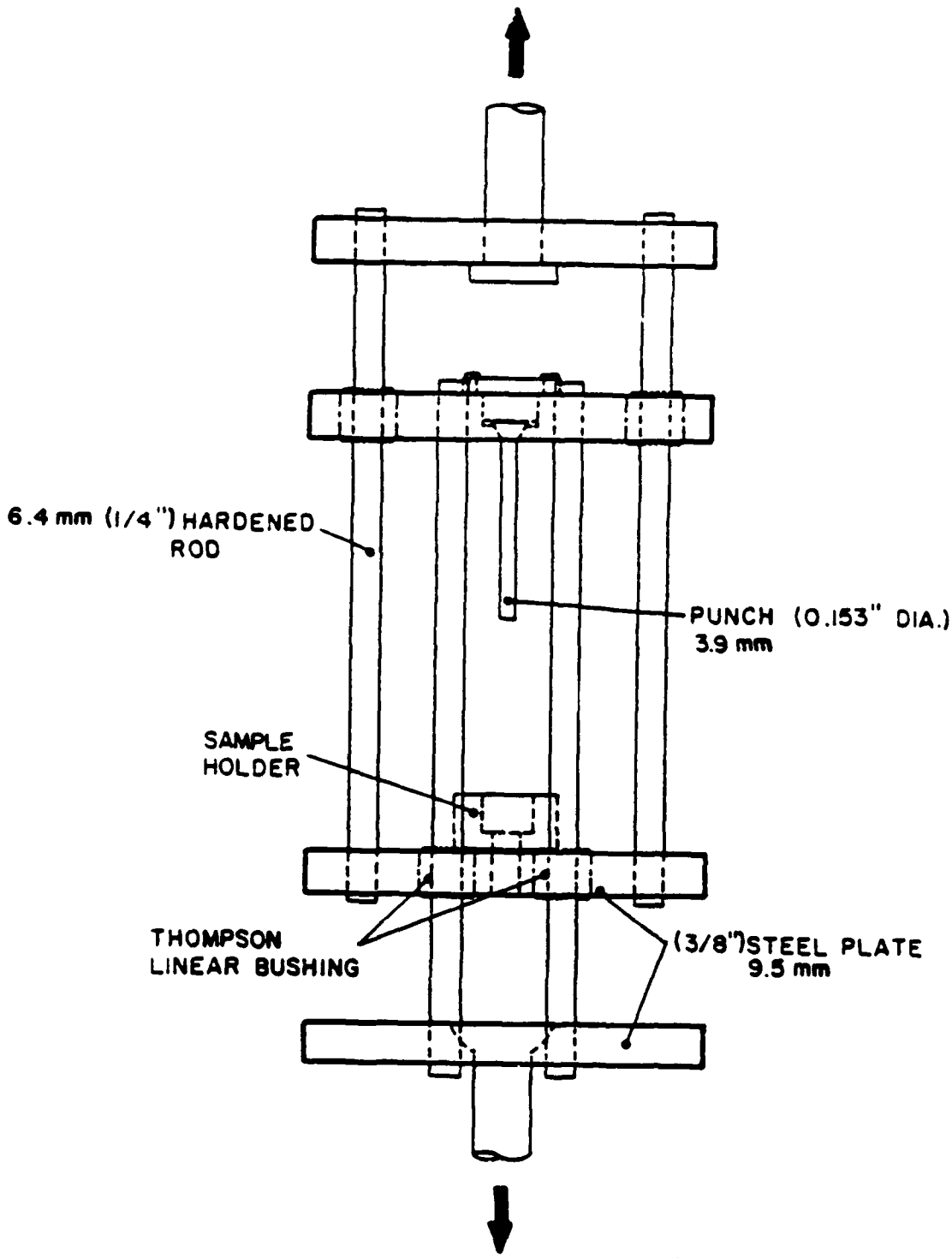

Figure 7. Schematic diagram of the jig used for punch shear tests.

chart recorder. The clearance between the punch and the die was approximately two percent; a schematic of the sample holder and die configuration is presented in Figure 8.

A cross-section of a sample for the punch shear test also is shown in Figure 8. Since one criterion of this test was to concentrate the shear stress at the metal/ceramic interface, it was important to prepare samples that could be aligned properly with respect to the punch and die. The SiC rod, punch, and tensile axis must all be parallel and perpendicular to the top surface of the die. Samples were carefully prepared to meet this criterion.

To prepare the sample disc, a SiC rod was submerged in molten aluminum, suspended in the metal for a given amount of time at temperature, and then frozen in place. The SiC rods were 99 wt. pct. pure sintered α-SiC from SOHIO. Since the as-received SiC rods were contaminated with a surface coating of carbon, the samples were first abraded with 600 grit emery cloth to remove the film, then ultrasonically etched for ~one hour in 20 pct. HF (by volume) at room temperature, and finally rinsed in methanol. The aluminum alloys were prepared and cast into graphite crucibles in an inert argon glove box. The purity of the aluminum, magnesium, and lithium metals, was $\geq$ 99.95 wt. pct.

To prepare a sample in the glove box, a 'cleaned' SiC rod was positioned along the axis centerline of the graphite crucible, and molten metal was poured into the crucible and around the SiC. The SiC rods extended at least one inch out of

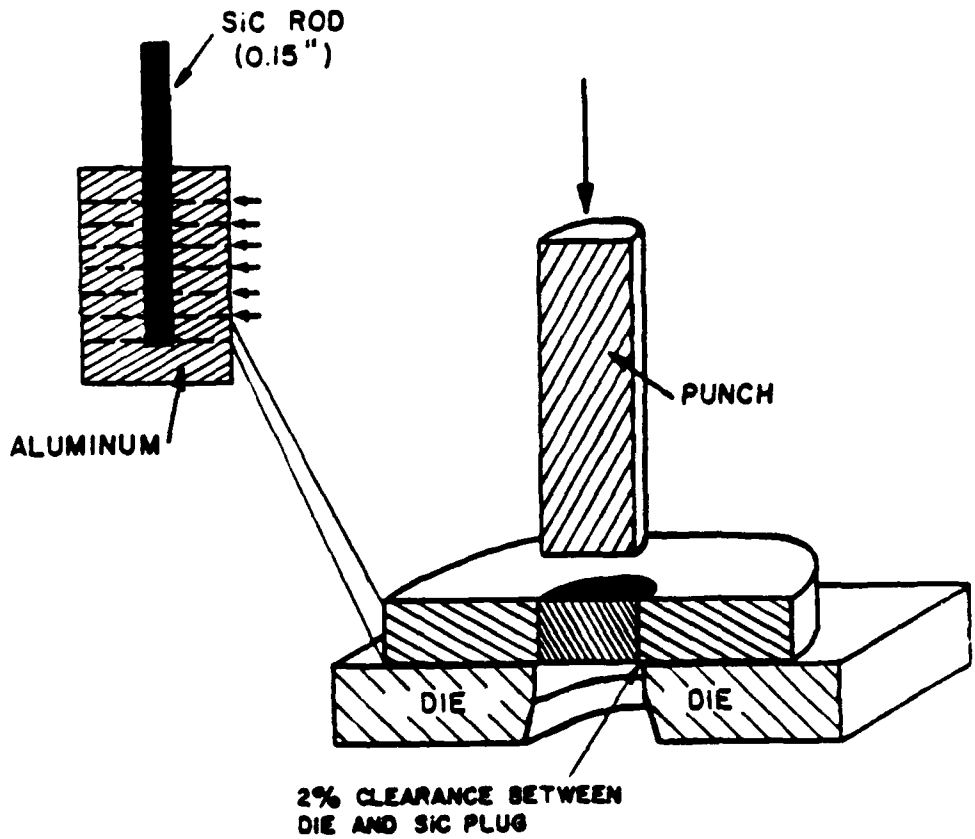

Figure 8. Schematic diagram of sample and die configuration.

the top of the crucible. The samples were then reheated to ~850°C and soaked for a given amount of time (i.e. 0, 20,45, or 90 minutes), insuring that the SiC rod was kept rigidly in place. After soaking, the samples were removed from the furnace and cooled in the argon atmosphere.

Cast and treated samples were sectioned perpendicular to the SiC rod axis on a diamond wafering saw, using the protruding SiC rod to clamp into the saw chuck. Since a target ratio of sample thickness to the punch diameter was previously established at 0.6 to 0.7, the samples were sectioned to a thickness of ~2.5 mm.

Once the sample was aligned and secured in the jig holder, the holder assembly was placed in the jig. The top hole of the holder was used as a guide to align the punch with the SiC plug. The punch rate, or cross head speed, was 0.13 cm/sec (0.05 in./min.). Bearing grease was applied to the punch to minimize frictional effects between either the die or the sample.

A 9080 kgf (20,000-lb) load cell was used in the Instron machine to handle the range of anticipated shear loads in the tests. The sensitivity of the low range was adequate for these tests.

5.3 Interfacial Strength of the Al/SiC Bond

A representative load-displacement curve from punch shear technique is shown in Figure 9. For those metal/ceramic interfaces where bonding was known to have developed (i.e., t=90 minutes), the measured shear load was found to increase linearly

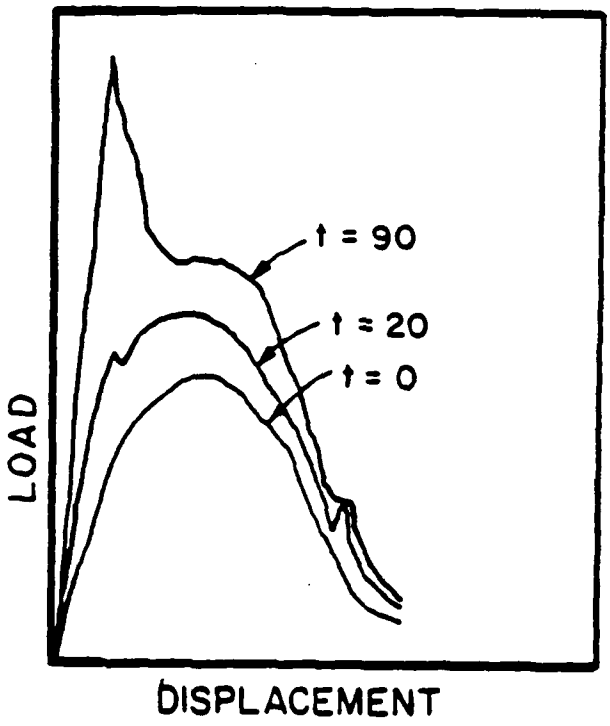

Figure 9. Punch shear test results, plotted as load diplacement versus reaction time in minutes.

to a characteristic point of instability. The remaining non-linear portion of the curve represents the process of pushing the SiC plug out of the aluminum matrix.

In the ideal case, this non-linear portion of the curve is due to frictional forces between the SiC and the aluminum; however, even the slightest misalignment between punch and sample can cause shearing in the matrix away from the interface and change the shape of the non-linear portion of the curve. The curves in Figure 9 represent the changes in observed behavior from purely frictional forces (no chemical bonding) to breaking of interfacial bonds (sharp transition at the instability point).

The initial inflection in the load-displacement curve, or point of instability, is a relative measure of the interfacial strength. To confirm this observation, samples were held at the reaction temperature for different lengths of time, t. At zero reaction time, an inflection did not occur in the curve and the observed shear stress was essentially a frictional stress. With increasing reaction times, the inflection point not only reappeared, but increased dramatically (refer to curves for 20 and 90 minutes). To a first approximation, the load at the instability point, divided by the interfacial area, was a relative measure of the interfacial strength. To more accurately quantify the interfacial bond strength, an attempt was made to measure the actual area of the reacted interface.

When examined with the scanning electron microscope (SEM), it was discovered that the SiC rod had only partially bonded to

the aluminum. This incomplete bonding was verified two ways. First, the morphology of the unreacted, sintered, SiC surface was found to be rough and porous, whereas the reacted SiC surface was smooth. Traces of sheared aluminum were generally left on those areas of the SiC surface that had reacted. In some cases, sheared aluminum was left on top of the bonded areas.

A second method of confirming the partial bonding at the interface was with energy dispersive x-ray (EDX) analysis. In the unreacted areas on the silicon carbide fracture surface, silicon was the only element detected. However, in the reacted areas, traces of aluminum were detected along with aluminum alloying elements, such as magnesium. On the mating, aluminum matrix fracture surface, the reacted areas of the fracture surface were found to contain traces of silicon.

In addition to these spot analyses for specific elements, a more extensive x-ray mapping was undertaken to quantify the fraction of bonding at the surface.

Using the SEM micrographs of the images and the EDX maps, the fractional areas were then determined with a LECO Image Analyzer. The results of this fractional area analysis are presented in Table 3. The 'average' under the X-RAY MAP heading refers to the average of the 'aluminum area' in the ALUMINUM X-RAY MAP and the 'non-silicon area' in the X-RAY MAP. After comparing the results from more than 25 x-ray maps and corresponding secondary electron images, it was apparent that

Table 3. Results of fractional bond area determination using Leco image analyser.

ALLOY	X-RAY MAP ALUMINUM	X-RAY MAP SILICON	AVERAGE	SECONDARY ELECTRON IMAGE
AL-MG (#106)	42.75	20.6	32	
	21.2	39.5	30	38.3
	7.5	35.1	21	24.2
	32.7	67.8	50	40
	13.6	67.8	41	40
		AVE:	35	36
Al-Mg (#104)	10.61	40.53	26	34
	10.03	50.1	30	34
	26.2	42.5	34	28.3
		AVE:	30	32
(group 1)		AVE:	48	
Pure Al	42	70.2	56	
	71.8	81.5	77	
		AVE:	66	
Al-Li (#204)	7.6	56	32	26.1
Al-Li (#202)	4			10.15

specific grey levels in these images would correspond to regions of bonding (darker) and non-bonding (lighter).

The procedure, therefore, for determining interfacial strengths was: 1) punch out the SiC from the aluminum matrix to measure the shear load, 2) quantify the fraction of interface bonding with SEM images and x-ray maps, and 3) normalize the shear strengths with respect to the fractional bond area.

5.4 Punch Shear Results (Al/SiC)

The results for the shear strengths of the pure aluminum/SiC couples are shown in Figure 10. Measured shear strengths (stress at instability point) versus reaction time at 850° are presented (solid points with error bars). These shear strengths are calculated assuming complete bonding at the interface (shear areas equal to surface area of SiC plug). Not surprisingly, these shear strengths were observed to increase with increased reaction or soak times at 850°C. Shear strengths appeared to reach a maximum and then level off after ~50 minutes, suggesting that increased carbide formation beyond a certain extent decreased the nominal shear strength of the interface.

The normalized strengths were calculated from the fractional bond area measurements and plotted in Figure 10 (adjusted points above the dashed line). Since the fraction of bond area increased with increased reaction time, the normalized shear strengths, for different reaction times, were all nearly the same.

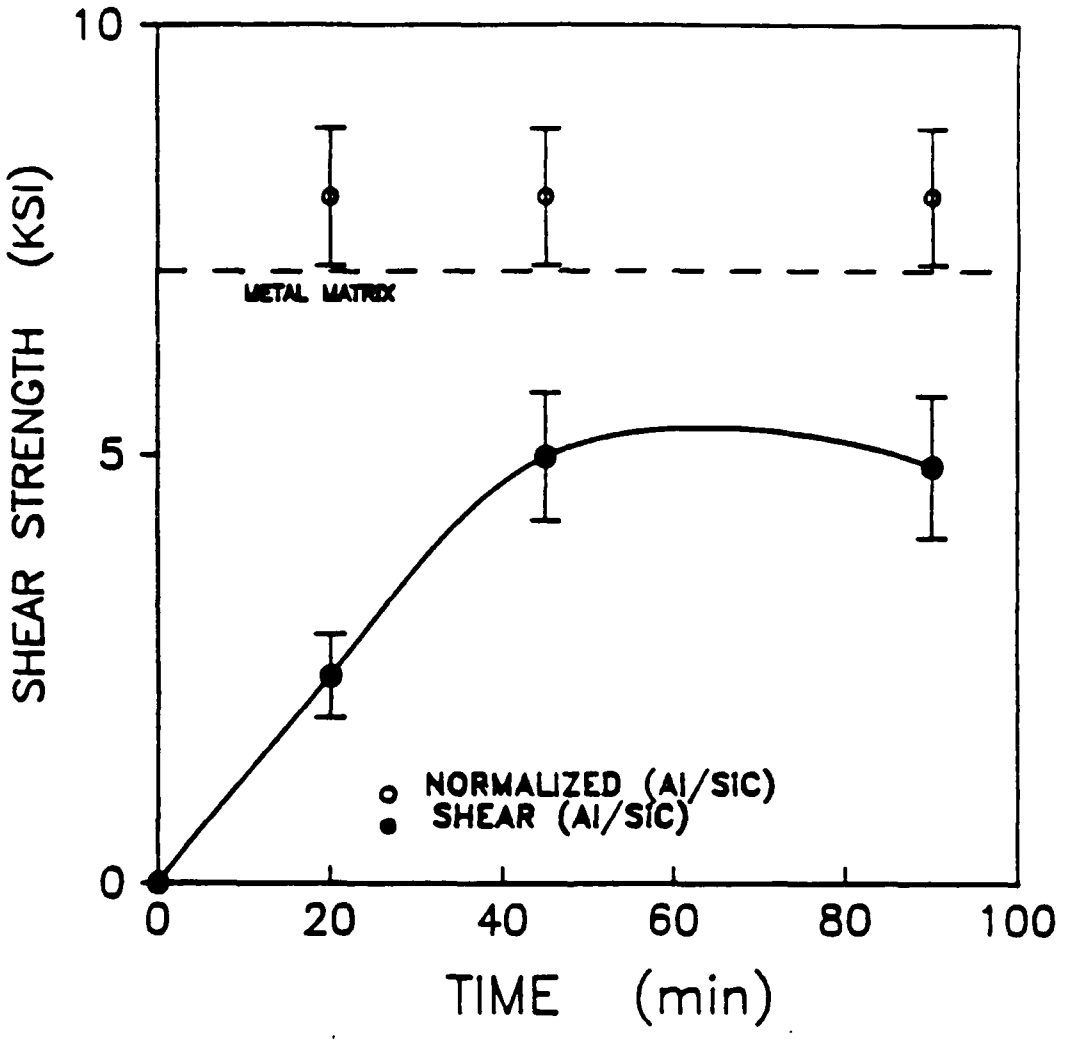

Figure 10. Bend strength versus reaction times in minutes for aluminum/silicon carbide couples.

The normalized interfacial shear strengths for pure aluminum/SiC were consistently higher than the measured shear strengths of the pure aluminum matrix (shown by the dashed line). The ratio of the normalized interfacial strength to matrix strength is equal to 1.2 (8550/7133), revealing that the binding energy of the aluminum matrix was less than the bonding energy between the aluminum and SiC at the interface.

Since solute strengthening is not present in pure aluminum, any increases in strength at the interface would result primarily from chemical interactions. The chemical interactions would involve aluminum, silicon, and carbon. It is well documented that pure aluminum reacts with SiC to form Al_4C_3.

It was possible to deduce the formation of a reaction product on the fracture surface. The morphology of the reacted surfaces were distinctly different from the unreacted surfaces. Specifically, the secondary electron images of the reacted areas were darker and more dense than those of the unreacted area. Fracture surfaces, where reaction had occurred, were dotted with fine powder remnants.

5.5 Comparison to Model (Pure Aluminum Matrix)

The decohesion model is discussed in terms of experimental results just presented. In the absence of any interaction between aluminum and silicon carbide, the work of decohesion would be equal to zero. Mathematically, this means that the magnitude of the interfacial energy, γ_{ss}, is equal to the sum of

the two surface free energies. As the metal and ceramic interact, the γ_{ss} term decreases and bonding occurs. The bond strength of the Al/SiC couple is therefore dependent upon the determination of the γ_{ss} term.

To calculate the interaction term, γ_{ss}, and subsequently the work of decohesion, the first step is to assume that aluminum carbide, Al_4C_3, was the primary reaction product at the interface. In this case, the enthalpy of formation, ΔH_f, is equal to 62.8 kcal/mole. The interaction term, γ_{ss}, is therefore equal to:

$$\gamma_{ss} = 2212\ [1-T/3500] - 1219 + 0.15\ (\gamma_{ss}^{A} + \gamma_{sv}^{B}) \qquad (13)$$

and the work of decohesion is equal to:

$$E_A = 0.85\ (\gamma_{sv}^{A} + \gamma_{sv}^{B}) - 0.361 = 2.19 J/m^2 \qquad (14)$$

where γ_{sv}(SiC) is equal to 1.8 J/m^2, and γ_{sv}(Al) is equal to 1.205 J/m^2.

The 2.19 J/m^2 is the calculated energy to separate the SiC from the aluminum (assuming formation of Al_4C_3). Since the experimental results are expressed in terms of a shearing force per unit area of interface, it is difficult to make an absolute comparison between the experimental strengths and the theoretical bond energies. To convert from a theoretical bond energy to a shear strength (force/unit area), an atomic separation, whether it be an interatomic spacing or potential barrier analogy, has to

be determined or assumed. For this study, a relative approach was adopted which compared the ratio of the interfacial bond energy (strength) to the pure metal matrix bond energy (strength). Relative changes in the interfacial bonds were referenced (or normalized) to the bonding in the pure metal matrix.

5.6 Punch Shear Results (Aluminum Alloy Matrix)

Two different aluminum-magnesium alloys, 3 and 7 at. pct. Mg, and two different aluminum-lithium alloys, 3.2 and 6.5 at. pct. Li, were reacted with SiC. In the first stage, all of the above alloys were reacted with SiC rods at 850°C for approximately twenty-minute soak times and then shear tested at room temperature. A second set of SiC rods were later exposed to specific molten alloys for longer periods of time to evaluate the effect of reaction time on the interfacial bond strength.

The results from these tests showed that there was no significant improvement in the normalized shear strengths for the aluminum-lithium alloys even after 80-minute reaction times. Since the measured shear strengths for the 80-minute tests were essentially the same as the 20-minute tests for the aluminum-lithium alloys, the results for the 20-minute tests are the only results presented in this discussion.

In the case of aluminum-magnesium alloys, increasing the reaction time from 20 to 60 minutes for the 3 at. pct. Mg alloy, had a dramatic effect on the experimental load-displacement

curve. The shear loads at the instability point for the 60-minute tests were more than three times greater than the previous 20-minute tests. In comparison to the shear loads for the pure aluminum samples, the un-normalized shear loads for the magnesium alloys were at least one and a half times greater. The instability points in the load-displacement curves for the 3 at. pct. Mg alloys were sharp and well defined.

5.7 Comparison to Model (Aluminum Alloy Matrix)

To calculate the interaction term, γ_{ss}, for the aluminum-magnesium case, an assumed chemical reaction or enthalpy of formation is needed. As a first approximation, the ΔH_f of a magnesium silicide, Mg_2Si, was substituted into the γ_{ss} expression. Using the free surface energies for aluminum-magnesium, and the calculated γ_{ss}, the theoretical interfacial bond energy was determined.

To compare the interfacial bond energy to the experimentally measured shear strengths, the interfacial energy was normalized with respect to the bond energy of the matrix. The theoretical matrix energy, using Equation 12, is equal to twice the free surface energy, γ_{sv}, of the aluminum alloy matrix (free surface energies from the proposed surface energy model). The theoretical ratio of interface/matrix bond energy was determined and the results are presented in Figure 11 (dashed line).

In comparison to the experimental line, the theoretical line for magnesium-bearing aluminum alloys in Figure 11 lies above the

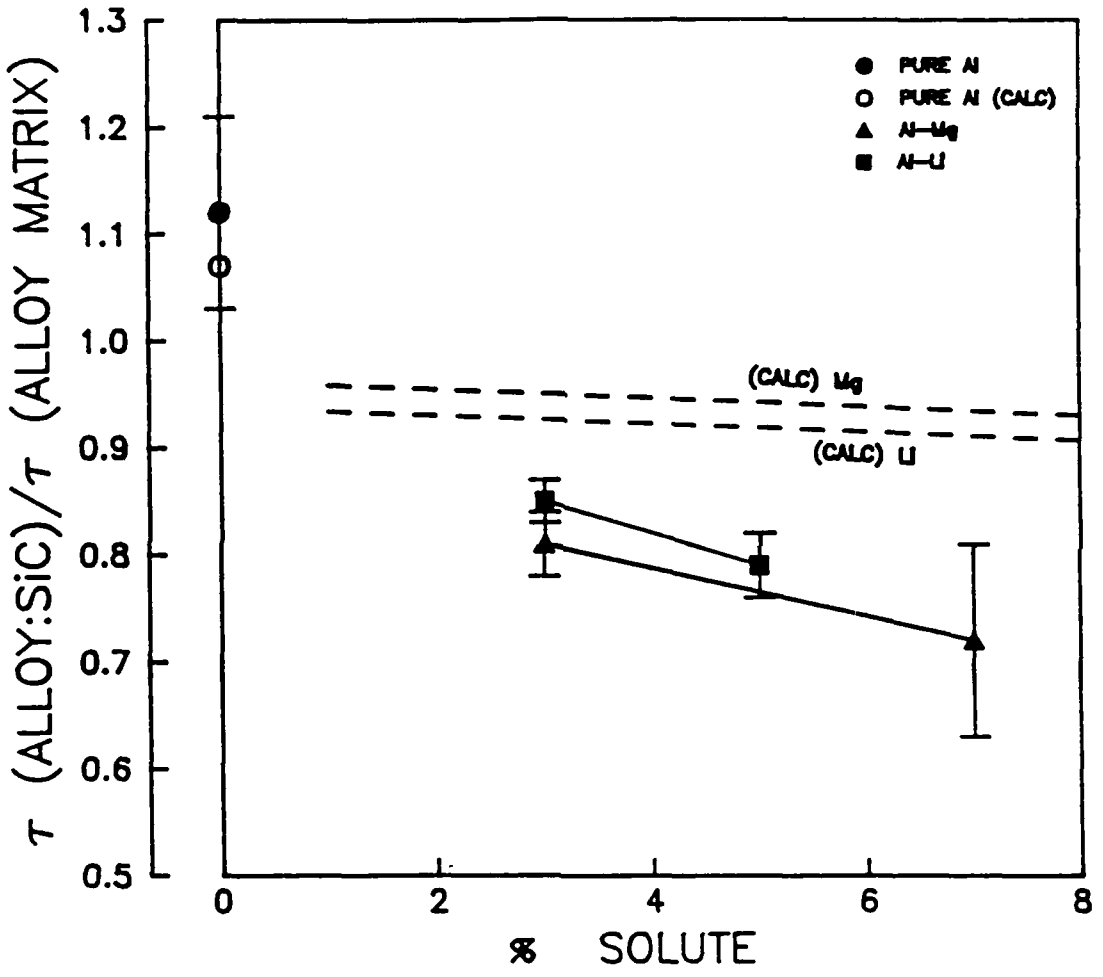

Figure 11. Comparison between theoretical and experimental bond strengths for aluminum-magnesium alloys.

experimental although the relative slopes are about the same. The experimental results for the Al-3 at. pct. Mg sample would place this point well above the theoretical line. The experimental ratios for the 60-minute, Al-3 at. pct. Mg specimens (although not shown in Figure 11) were much greater than one (~1.5). If it is assumed that a stable compound such as an Al_2MgO_4 or Mg_2SiO_4 spinel formed at the longer, 60-minute reaction time, then the theoretical ratio would be of the same order of magnitude as the experimental ratio for the 60-minute test (the ΔH_f of a spinel was substituted into the γ_{ss} equation). The position of the Al-Mg theoretical line, as shown here, is ultimately dependent on the choice of interfacial reaction; the most thermodynamically stable compound being preferentially selected.

Independent of the nature of the chemical compounds forming, it was observed, for a given reaction time, that increased magnesium concentrations did not proportionately increase the strength of the interface. Increasing magnesium concentrations in fact decreased slightly the strength of the interface as compared to the strength of the matrix.

The calculated interface/matrix ratios for different lithium additions, are plotted in Figure 11 (dashed line). As in the aluminum-magnesium case above, the interface and matrix energies were calculated from equation (11), the work of decohesion. The experimental optical transition energies and surface free energy model were used in calculating the free surface energies. Since

it was assumed that no reaction product formed at the interface (i.e. $\Delta H_f=0$), the calculated decrease with increasing lithium concentration was the result of the decrease in free surface energies in the E_a equation (12a). The work of decohesion, E_a, correctly predicted the observed trend shown in Figure 11.

It should be re-emphasized that the proposed bonding model is based on chemical interactions, and strengthening from mechanical effects are neglected. The objective in this study though, was to attempt to predict properties in terms of a chemical model and later incorporate other effects, such as mechanical strengthening. Because of the complexity of the solid/solid interface, in comparison to the solid/liquid interface, a bonding model; may have to incorporate both the chemical and mechanical effects.

6.0 REFERENCES

1. Edwards, G.R., and Olson, D.L., "Investigation into the Infiltration Kinetics and Interfacial Bond Strength of Aluminum/Silicon Carbide Composites", Annual Report No. MT-CWR-088-022, Colorado School of Mines, July, 1988.

2. Edwards, G.R., and Olson, D.L., "Investigation into the Infiltration Kinetics and Interfacial Bond Strength of Aluminum/Silicon Carbide Composites", Annual Report No. MT-CWR-089-038, Colorado School of Mines, July, 1989.

3. Phillips, J.C., and Van Vechten, J.A., "Spectroscopic Analysis of Cohesive Energies and Heats of Formation of Tetrahedrally Coordinated Semiconductors", Phys. Review B, Vol. 3, pp. 445 (1954).

4. Hummel, R.C., and Nastas-Andrews, R.J., "Optical Properties and Electronic Structure of Dilute Cu-Au, Cu-Zn, Cu-Al, Cu-Ga, Cu-Si, Cu-Gi, Cu-Sn, and Cu-As Alloys", Phys. Rev. B., vol. 16, no. 10, p. 4314, (1977).

5. Benbow, R.L., and Lynch, D.W., "Optical Absorption in Al Dilute Alloys of Mg and Li in Al at 4.2°K", Phys. Rev. B., vol. 12, no. 12, (1975), p. 307.

6. Takai, T., Halicioglu, T., Tillar, W.A., "Reconstruction and Energetics for Surface of Silicon Diamond, and B-SiC", Surf. Sci., vol. 164, p. 341, (1985).

7. MacKrodt, W.C., "Calculated Point Defect Formation, Association, and Migration Energies in MgO and α-Al_2O_3", Advances in Ceramics, vol. 10, American Ceramics Society.

8. Janef Thermochemical Tables, 2nd Ed., (1977), U.S. Dept. of Commerce.

9. Overbury, S.A., Bertrand, P.A., and Somorjai, G.A., "The Surface Composition of Binary Systems Predictions of Surface Phase Diagrams of Solid Solutions", Chemical Reviews, vol. 75, no. 5, p. 547, (1975).

10. Murr, L.W., "Interface Phenomena in Metals and Alloys", Addison Wesley Publishing Co., Mass., p. 376, (1975).